Derivation of algorithms for phase-shifting interferometry using the concept of a data-sampling window

Peter de Groot

I propose a systematic way to derive efficient, error-compensating algorithms for phase-shifting interferometry by integer approximation of well-known data-sampling windows. The theoretical basis of the approach is the observation that many of the common sources of phase-estimation error can be related to the frequency-domain characteristics of the sampling window. Improving these characteristics can therefore improve the overall performance of the algorithm. Analysis of a seven-frame example algorithm demonstrates an exceptionally good resistance to first- and second-order distortions in the phase shift and a much reduced sensitivity to low-frequency mechanical vibration.

1. Introduction

An effective means of profiling smooth surfaces interferometrically is to analyze a sequence of fringe patterns shifted in phase with respect to each other.[1,2] Phase-shift interferometry (PSI) is capable of high resolution, provided that the instrument is properly adjusted and is in a quiet environment. On the other hand, seemingly slight errors in phase shifting can result in significant measurement errors. Other familiar difficulties include sensitivity to vibration, especially the low-frequency vibration common in production environments.

It has been known for some time that the performance of a PSI instrument is greatly affected by the choice of the phase-demodulation algorithm.[3] Until recently, an overriding concern in surface metrology was the amount of memory required to store camera frames temporarily and the speed of data processing, so the figure of merit for a PSI algorithm was its brevity. The best PSI algorithm was therefore the one that used the least amount of data. For many years, the most common algorithms used only three or four camera frames to calculate phase. Unfortunately, the shortest algorithms are also the ones that are most sensitive to intensity noise, mechanical vibration, and errors in phase shifting. Hence the folklore concerning optimization of these hardware-related characterizations of the instrument.

Improvements in computing power together with increasing demands on performance are encouraging instrument designers to look into PSI algorithms that use more data points but are at the same time more resistant to environmental problems and system errors. The thesis of this paper is that many of the problems of PSI, such as sensitivity to variations in the data-sampling interval, are related to the fact that many PSI algorithms use a rectangular data window. When the data are analyzed for phase, it is found that the result is easily corrupted by intensity noise at frequencies far removed from the basic modulation frequency of the interferometer. Thus one possible way to enhance performance is to derive new algorithms based on windowing functions that improve the frequency response characteristics of PSI.

The objective here is to provide a systematic means for deriving computationally efficient PSI algorithms that are tolerant of phase-shift errors and vibrational noise. The foundation for the derivation is the somewhat unusual description of PSI in terms of data-sampling windows and Fourier transforms. This approach reveals the importance of the window and provides a means of deriving new algorithms of almost any length and phase increment. After describing the derivation method in general terms, I present extensive analysis and experimental testing of a new algorithm based on seven camera frames of intensity data.

2. Theory

When PSI algorithms were restricted to combinations of three or four intensity values, the choice of algorithm was also restricted to those combinations

The author is with Zygo Corporation, Laurel Brook Road, Middlefield, Connecticut 06455.

Received 20 May 1994; revised manuscript received 29 September 1994.

0003-6935/95/224723-08$06.00/0.

that were reasonably independent of fringe contrast and intensity bias. However, the number of possible algorithms using five or more intensity values requires a more systematic approach to their design and assessment. A good algorithm should be not only resistant to phase-shift errors but should also be computationally efficient and relatively easy to implement with existing instrumentation.

An example of intelligent algorithm design is the averaging method introduced by Schwider *et al.*[4] This method compensates the effect of phase-shift calibration error by effectively summing the results of two consecutive measurements separated by $\pi/2$ in phase. Currently, the most widely used PSI algorithm in surface metrology is the Schwider–Hariharan five-frame algorithm, which can be derived by averaging two four-frame algorithms.[4,5] A variety of algorithms can be generated by repeated application of $\pi/2$ averaging.[6]

A more recent trend in algorithm design follows from the Fourier description introduced by Freischlad and Koliopoulos.[7] The basic idea is to picture PSI as a filtering process in the frequency domain and to analyze the various algorithms according to their frequency response. Larkin and Oreb have developed a procedure for deriving a special class of symmetrical PSI algorithms using Fourier analysis as a guide.[8] The frequency-domain picture has considerable appeal, since it has the potential of providing a more general approach to algorithm development than previous methods.

In this section I outline a general PSI theory that is also based on Fourier analysis, with the principal novelty being the emphasis on the use of well-known transform windows. The central task of PSI is to estimate the interference phase θ, which is linearly proportional to an object distance or surface height, by inspection of a time-dependent periodic signal $g(\theta, t)$. In a two-beam interferometer, the signal corresponding to a single image point in the fringe pattern is given by

$$g(\theta, t) = Q[1 + V\cos[\theta + \phi(t)]], \tag{1}$$

where V is the fringe visibility, Q is a constant, and $\phi(t)$ is the phase shift. Since this signal is periodic, one way to determine phase θ is to transform the signal $g(\theta, t)$ into the frequency domain:

$$G(\theta, \nu) = \int_{-\infty}^{\infty} g(\theta, t)w(t)\exp(-i2\pi\nu t)\mathrm{d}t. \tag{2}$$

Phase θ can then be extracted by comparing the imaginary and real parts of the strongest coefficient $G(\theta, \nu)$ in the frequency-domain representation of the interference signal.[9,10] The window function $w(t)$ is included to reduce the spectral leakage associated with finite observation intervals. Although this is not the usual way of describing PSI, almost any PSI algorithm may be put in the form of Eq. (2), with the variety in the form of the algorithm being due primarily to the flexibility in choice of the window function $w(t)$.

The description of PSI in terms of Eqs. (1) and (2) is very broad and covers a great number of data acquisition and processing schemes, including pseudorandom phase shifts, two-frequency heterodyne interferometry, discrete sampling, and so on. To narrow the range of possible algorithms, let us first assume that the phase shift is continuous and approximately linear, so that

$$\phi(t) \approx 2\pi\nu_0 t. \tag{3}$$

The Fourier transform in this case evaluates to

$$G(\theta, \nu) = Q[W(\nu) + \tfrac{1}{2}V[W(\nu - \nu_0)\exp(i\theta) + W(\nu + \nu_0)\exp(-i\theta)]], \tag{4}$$

where $W(\nu)$ is the Fourier transform of the window function $w(\nu_0)$. If the window is constructed so that

$$W(\nu_0) = 0, \tag{5}$$

$$W(2\nu_0) = 0, \tag{6}$$

then

$$\theta = \tan^{-1}(T) + \text{const}, \tag{7}$$

where

$$T = \frac{\mathrm{Im}[G(\theta, \nu_0)]}{\mathrm{Re}[G(\theta, \nu_0)]}, \tag{8}$$

and the constant is the complex phase of the transformed window at $\nu = 0$. This is the essential result for the hypothetical case of a continuous signal.

In practice, PSI often involves an approximation of discrete sampling based on a sequence of a few integrated intensity values. In a surface-measuring instrument, each intensity sampling j corresponds to a frame of camera data. For the discrete case, there are a series of phase shifts ϕ_j such that

$$w(\theta, t) = \sum_j w_j\delta[t - (\phi_j/2\pi\nu_0)], \tag{9}$$

where $\delta[\,]$ is the Dirac delta function. The actual sampling may in fact involve data integration between the sampling increments, but, for the present purpose, the effects of this integration may be included in the measured signal. The Fourier transform of the discretely sampled intensity is

$$G(\theta, \nu_0) = \sum_j g_j w_j \exp(-i\phi_j). \tag{10}$$

The ratio defined in Eq. (8) becomes

$$T = \sum_j s_j g_j \Big/ \sum_j c_j g_j, \tag{11}$$

where

$$s_j = \mathrm{Im}[w_j \exp(-i\phi_j)], \tag{12}$$

$$c_j = \mathrm{Re}[w_j \exp(-i\phi_j)]. \tag{13}$$

The inverse calculation is also possible. If we know the coefficients s_j and c_j, the window weights w_j are

$$w_j = [s_j \sin(-\phi_j) + c_j \cos(\phi_j)] + i[s_j \cos(\phi_j) - c_j \sin(-\phi_j)]. \tag{14}$$

Equation (14) is useful when existing algorithms are evaluated.

The conditions in Eqs. (5) and (6) for the discrete case reduce to familiar forms. Equation (5) is the result of the dc term in the intensity function and is satisfied by

$$\sum_j s_j = 0, \qquad \sum_j c_j = 0. \tag{15}$$

Equation (6) requires that the leakage from the negative-frequency portion of the spectrum should go to zero at the modulation frequency. In the discrete case, this condition requires the simultaneous satisfaction of the following two equations:

$$\sum_j s_j \sin(-\phi_j) = \sum_j c_j \cos(\phi_j), \tag{16}$$

$$\sum_j s_j \cos(\phi_j) = -\sum_j c_j \sin(-\phi_j). \tag{17}$$

Further simplifications are possible for the special case of a symmetric, real window function $w(t)$. For this special case,

$$s_j = w_j \sin(-\phi_j), \tag{18}$$

$$c_j = w_j \cos(\phi_j). \tag{19}$$

Although the general formalism provided here is not limited to real, symmetric windows, it turns out that this is a useful class of algorithms.

3. Algorithm Design

Poor performance in PSI can most often be traced to problems in satisfying Eqs. (5) and (6) in various situations that deviate from the ideal case.[11] When Eqs. (5) and (6) are not completely satisfied, the additional terms in Eq. (4) arising from the dc bias and the negative-frequency Fourier signal contribute to measured phase. In particular, when $W(2\nu_0) \neq 0$ there will be a periodic error at two times the modulation frequency of the phase shift. Thus in a well-designed algorithm, the Fourier transform $W(\nu)$ of the window function should be close to zero over as large a range as possible, especially in the neighborhood of $\nu = 2\nu_0$. From these observations we can conclude that one way to enhance the performance of PSI is to use windowing concepts to adjust the graphic appearance of $W(\nu)$.

The digital filtering and signal processing literature provides a wide variety of data windows for improving frequency and phase estimation.[12,13] Generally these windows are real and symmetric and are designed to reduce the amount of high-frequency ripple in the Fourier transform, at the expense of a somewhat broadened sensitivity around $\nu = 0$. Consider, for example, the two windows and their Fourier transforms shown in Figs. (1) and (2). The first window is a simple rectangular function that represents a uniform data sampling over a range of phase shifts. The Fourier transform of this window exhibits the appropriate zero points at $\nu = \nu_0$ and $\nu = 2\nu_0$, but there are strong derivatives in the neighborhoods of these points. A PSI algorithm based on this window would be sensitive to changes in the modulation frequency and to low-frequency intensity noise. On

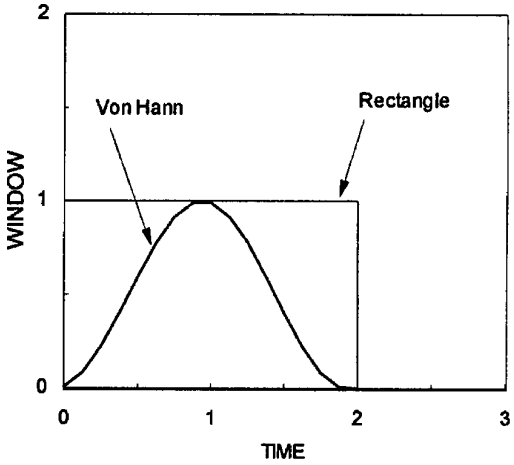

Fig. 1. Comparison of two data-sampling windows. The time scale is normalized to the period of the fundamental phase-shift frequency ν_0. As the number of data samples increases, it becomes increasingly more practical to design integer-math PSI algorithms that approximate a Von Hann window.

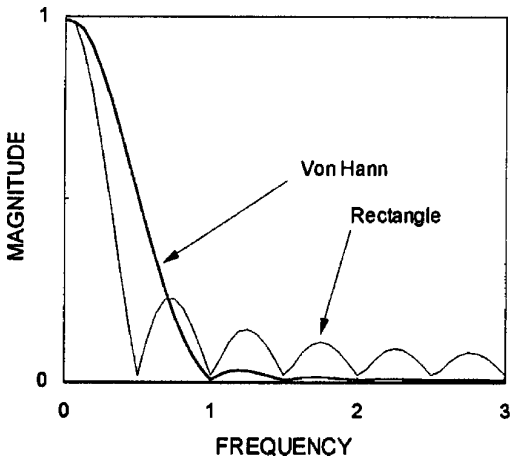

Fig. 2. Positive-frequency portions of the Fourier transforms of the windows shown in Fig. 1. The frequency-space graph shows rapid variations around $\nu = 2\nu_0$ for the rectangular window, which in practice results in high sensitivity to phase-shift errors. The transform of the Von Hann window, on the other hand, is relatively flat in the neighborhood of $\nu = 2\nu_0$, resulting in improved performance.

the other hand, the window shown in Fig. 2 has much better behavior in the frequency domain, particularly in the neighborhood of $\nu = 2\nu_0$.

The nonrectangular window shown in Fig. 1 is commonly known as a raised cosine or Von Hann window, and it has the functional form

$$w_j = 0.5 + 0.5 \cos\left[\frac{2\pi}{P'}\left(j - \frac{P}{2}\right)\right], \tag{20}$$

where P is the number of data samples, $j = 0 \ldots P - 1$, and P' is the window width. From basic notions of the discrete Fourier transform we know that the effective length of the data sample is of critical importance. Generally it is desirable to have the sample length be an integer multiple of the fundamental signal period, so that, at least in the ideal case, the signal will project into a single frequency of the spectrum. This condition is satisfied for the exact form of the window by

$$P' = N\frac{2\pi}{\alpha}, \tag{21}$$

where N is an integer and α is the phase increment.

An exact representation of this window requires that $P = P' - 1$ and most likely the manipulation of noninteger or even irrational numbers. However, from a computational point of view, it is desirable to work with integer coefficients s_j and c_j. This imposes an approximation to the ideal case, represented by the formulas

$$s_j = \text{round}[Xw_j \sin(-\phi_j)], \tag{22}$$

$$c_j = \text{round}[Xw_j \cos(\phi_j)], \tag{23}$$

where round[ ] is a function that returns the nearest integer to its argument, and X is chosen to provide a good approximation of the window. The necessary phase shifts are

$$\phi_j = \left(j - \frac{P-1}{2}\right)\alpha, \tag{24}$$

where $P \leq P' - 1$ is the number of nontrivial data samples required for Eqs. (22) and (23). When selecting a suitable scaling factor, it is important to verify by direct computation that Eqs. (5) and (6) are satisfied.

Some example algorithms derived from an integer approximation to the Von Hann window are shown in Table 1. These examples are found by a simple computer search for scaling values X such that there is a good fit to the exact window while at the same time the coefficients satisfy Eqs. (15) and (16). Four of the examples are based on a $\pi/2$ phase increment, which is the most widely used in PSI systems. The three other examples have $2\pi/3$, $\pi/3$, and $\pi/4$ phase increments to illustrate that the method is not limited to any particular phase-shift procedure. It is worthwhile noting that it is possible to have computationally efficient integer-math algorithms even when the phase increment is not equal to $\pi/2$.

It is also possible to recast the Schwider $\pi/2$ averaging technique[4] in terms of data-sampling windows and obtain many of the same results. Given a set of P window coefficients w_j satisfying Eqs. (5) and (6) for a $\pi/2$ phase increment, an improved window $\tilde{w}_j$ having $P + 1$ weights can be constructed from

$$\tilde{w}_j = w_j + w_{j-1}, \tag{25}$$

where $j = 0 \ldots P$ and $w_j = 0$ outside the range of $0 \ldots P - 1$. A simple four-frame algorithm, for example, has the square window $w_j = 1$ for $j = 0 \ldots 3$. A five-frame window calculated from Eq. (25) has coefficients $\tilde{w}_0 = \tilde{w}_4 = 1$ and $\tilde{w}_1 = \tilde{w}_2 = \tilde{w}_3 = 2$, which in fact is the data-sampling window for the Schwider–Hariharan five-frame algorithm referred to in Section

Table 1. Examples of Algorithms Derived from an Integer Approximation to the Von Hann Window

P	P'	α	X	T
5	8	$\pi/2$	2	$\frac{2(g_2 - g_4)}{-(g_1 + g_5) + 2g_3}$
6	8	$\pi/2$	6	$\frac{-(g_0 - g_5) - 3(g_1 + g_4) + 4(g_2 - g_3)}{-(g_0 + g_5) + 3(g_1 - g_4) + 4(g_2 + g_3)}$
7	8	$\pi/2$	8	$\frac{-(g_0 - g_6) + 7(g_2 - g_4)}{-4(g_1 + g_5) + 8g_3}$
11	12	$\pi/2$	16	$\frac{(g_0 - g_{10}) - 8(g_2 - g_8) + 15(g_4 - g_6)}{4(g_1 + g_9) - 12(g_3 + g_7) + 16g_5}$
8	9	$2\pi/3$	20	$\frac{2(g_0 - g_7) - 7(g_1 - g_6) + 17(g_3 - g_4)}{(g_0 + g_7) + 4(g_1 + g_6) - 15(g_2 + g_5) + 10(g_3 + g_4)}$
8	12	$\pi/3$	2.7	$\frac{-g_0 + g_1 + g_3 - g_4 - g_6 + g_7 + 2(g_2 - g_5)}{-(g_0 + g_1 + g_6 + g_7) + 2(g_3 + g_4)}$
9	16	$\pi/4$	2	$\frac{g_1 + g_3 - g_5 - g_7 + 2(g_2 - g_6)}{-g_0 - g_1 + g_3 + g_5 - g_7 - g_8 + 2g_4}$

2. Successive application of Eq. (25) also leads to the $P = 5, 6, 7$ examples for $\alpha = \pi/2$ in Table 1.

As a final note, it should be clear that multiplying the window by an overall complex constant of unit magnitude does not change the fundamental properties of the window in the frequency domain but simply introduces an asymmetry in the data-sampling that is equivalent to adding a constant phase offset to the data shifts ϕ_j in Eq. (24). This means that we are free to include such a phase shift in order to simplify the final appearance of the algorithm. For example, by multiplying the Von Hann window by $\exp(-i\pi/4)$ and using an integer approximation to Eqs. (12) and (13), the $P = 6$ algorithm in Table 1 simplifies to

$$T = \frac{3g_1 - 4g_3 + g_5}{-g_0 + 4g_2 - 3g_4}. \tag{26}$$

Apart from the $\pi/4$ phase shift, this asymmetric $P = 6$ algorithm has the identical data-sampling window as the symmetric version and has the same dynamic response.

4. Seven-Frame Algorithm

From the point of view of insensitivity to phase-shift errors, vibration, and intensity noise, the best algorithms overall are typically those that have the closest fit to an exact analytical window. Various criteria can be established for determining the goodness of fit, but, as a rule of thumb, we should expect that the best algorithms will have a number P of nontrivial data samples close to the window width P'. Looking at Table 1, it can be seen that there is a progressively better fit to the $P' = 8$ Von Hann window as the number of data samples P increases from 5 to 7. Thus we should expect that the $P = 7$ will provide the best approximation to the analytical window. In this section, I compare the relative performance of the seven-frame algorithm with that of the five-frame algorithm, using assessment techniques independent of the window theory.

The seven-frame algorithm in Table 1 determines interferometric phase θ using

$$\theta = \tan^{-1}(T), \tag{27}$$

where

$$T = \frac{7(g_2 - g_4) - (g_0 - g_6)}{-4(g_1 + g_5) + 8g_3}. \tag{28}$$

The intensity values g_j correspond to phase shifts given by

$$\varphi_j = (j - 3)(\pi/2), \tag{29}$$

where $j = 0 \ldots 7$. Computationally, the seven-frame algorithm has much in common with the Schwider–Hariharan five-frame algorithm, which appears in Table 1 as the $P = 5$ approximation to the same window function. The difference between the five- and seven-frame algorithms is the extra term $(g_0 - g_6)$ and some overall scaling factors. These small differences have a significant effect on the resulting performance.

The most important benefits of the seven-frame algorithm are excellent resistance to distortions in the phase shift, and reduced sensitivity to low-frequency mechanical vibration. The effect of phase-shift errors will be considered first. Suppose that instead of uniform, equidistant phase shifts as in Eq. (29), we instead have

$$\varphi_j = \left[\frac{\pi}{2} - \epsilon + (j - 3)\gamma\right](j - 3), \tag{30}$$

where ϵ and γ are first- and second-order distortion coefficients, respectively. The first-order distortion could be due to a calibration error in the phase shift, and the second-order distortion is common in both the motion of piezoelectric transducer (PZT) actuators and the wavelength-tuning response of laser diodes.

The effect of a distorted phase shift of this kind can be predicted to good accuracy by inserting Eq. (30) into Eq. (28), propagating the error through Eq. (27), and expressing the result as a Taylor series expansion for small ϵ and γ. This procedure leads to the following analytical expression for the phase error $\Delta\theta$ for the seven-frame algorithm in the presence of distortions in the phase shift:

$$\Delta\theta_{\text{seven}} = 2\gamma - (3\gamma^2/4)\sin(2\theta) + (\epsilon^4/16)\sin(2\theta) + \cdots. \tag{31}$$

Note that, for simplicity, the cross terms between the two error sources are not shown in Eq. (31). For comparison, it is useful to perform the same analysis with the five-frame algorithm. The result for this case is

$$\Delta\theta_{\text{five}} = 3\gamma/2 - (\gamma/2)\cos(2\theta) + (\epsilon^2/4)\sin(2\theta) + \cdots. \tag{32}$$

The important difference between these results is that the terms periodic in 2θ have a smaller amplitude for the new seven-frame algorithm when compared with the five-frame algorithm.

The effect of a first-order distortion is shown graphically in Fig. 3. The horizontal axis is the relative calibration error and is equal to the ratio of ϵ to $\pi/2$, the nominal shift increment. The vertical axis is the predicted P–V error resulting from the oscillatory terms in Eqs. (31) and (32). The phase measurement error is effectively eliminated with the new algorithm. This insensitivity to overall phase-shift calibration can be important in fast spherical cavities, even with a perfectly calibrated phase-shifting device.[12,14]

The effect of second-order distortions in the phase shift is shown graphically in Fig. 4. The horizontal axis is the amount of quadratic nonlinearity, defined

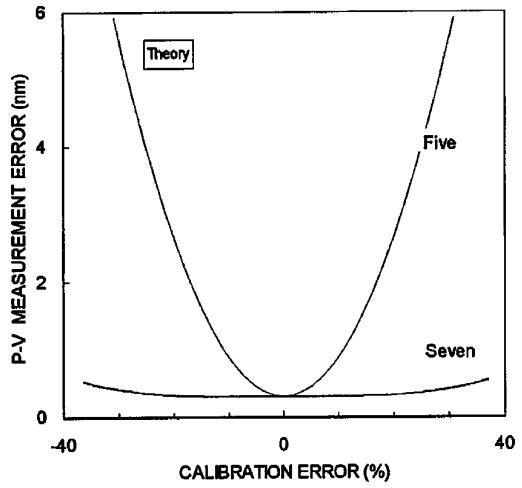

Fig. 3. Theoretical P–V surface measurement error in PSI that is due to miscalibration of the phase shift. The graph compares the seven-frame algorithm in Table 1 with the Schwider–Hariharan five-frame algorithm for an illumination wavelength of 600 nm. An arbitrary offset of 0.3 nm has been added to both curves.

here as the ratio of γ to $\pi/2$. From this graph it is clear that, with conventional PSI algorithms, nonlinearities can contribute significant errors to the phase measurement. The reduced sensitivity to quadratic nonlinearities makes it possible to use inherently nonlinear phase-shift devices, such as low-voltage PZT actuators and tunable laser diodes, without loss of accuracy.[15]

Many high-quality interferometric instruments have linear, well-calibrated phase shifts and there may appear to be little benefit in using algorithms that require more data frames. However, even in the case of a well-calibrated instrument, there can be environmental factors that degrade the system accuracy. Perhaps the most significant of these is vibration. Small-amplitude vibrations during a measurement result in phase-measurement errors $\Delta\theta$ composed principally of an offset constant over the field of view and an additional term periodic in 2θ.

Recent research has shown that the sensitivity to vibration is closely related to the type of PSI algorithm, and this vibrational sensitivity can be predicted in detail using a linear approximation and Fourier transform methods.[16–18] The Fourier approach is a relatively straightforward way to evaluate analytically the new algorithm for sensitivity to vibration. Suppose, for example, that we have a single vibrational tone of frequency ν and amplitude A_0. Using the formalism developed in Refs. 17 and 18, we find that the rms expectations of the resulting periodic phase error for the five- and seven-frame algorithms are

$$E_{\text{seven}} = A_0\left|\frac{\cos(\nu\pi/2)\sin^2(\nu\pi/4)}{2} + \frac{\cos(3\nu\pi/2) - \cos(\nu\pi/2)}{32}\right|, \tag{33}$$

$$E_{\text{five}} = A_0\left|\frac{\cos(\nu\pi/2)\sin^2(\nu\pi/4)}{2}\right|. \tag{34}$$

Equations (33) and (34) are plotted in Fig. 5. These curves are drawn as a function of the vibrational frequency for a camera frame rate of 60 Hz. The vibrational sensitivity plotted in Fig. 5 is nearly the same for the two algorithms at frequencies of 30 and 90 Hz. However, between these frequencies and particularly in the low-frequency region there are significant differences. The new algorithm dramatically improves the low-frequency behavior. Low-frequency vibrations correspond to gentle air cur-

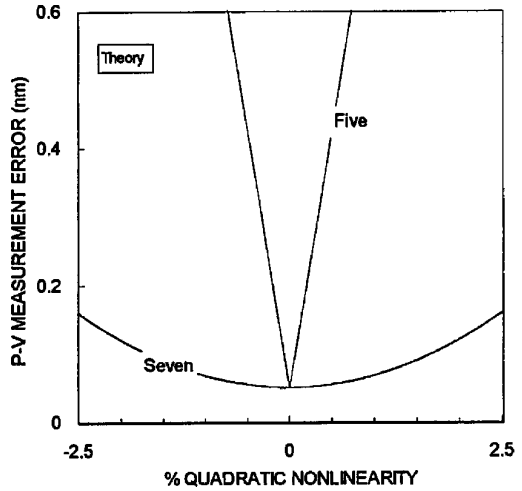

Fig. 4. Theoretical P–V surface measurement error in PSI that is due to quadratic nonlinearities in the phase shift. The graph compares the seven- and five-frame algorithms for an illumination wavelength of 600 nm.

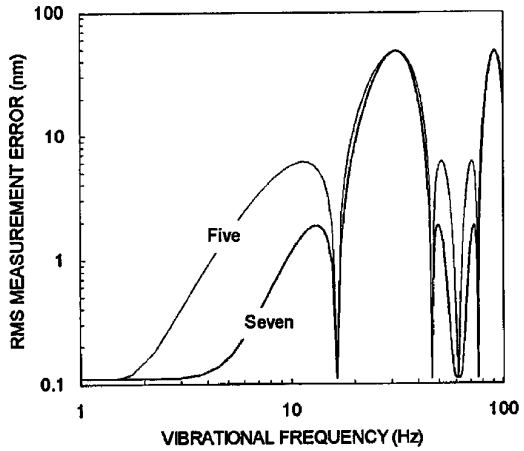

Fig. 5. Theoretical rms surface measurement error in PSI that is due to mechanical vibration during the measurement. The graph compares the sensitivity of the seven- and five-frame algorithms as a function of vibrational frequency. An arbitrary offset of 0.11 nm has been added to both curves.

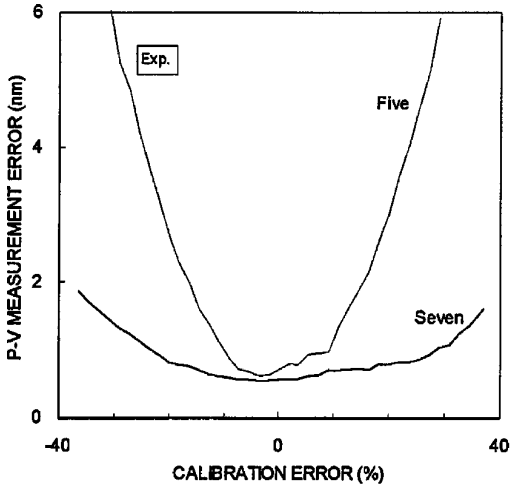

Fig. 6. Experimental P–V surface measurement error in PSI that is due to a deliberate miscalibration of the phase shift. These data were obtained with a white-light interferometric microscope and a mean illumination wavelength of 600 nm. Compare with Fig. 3.

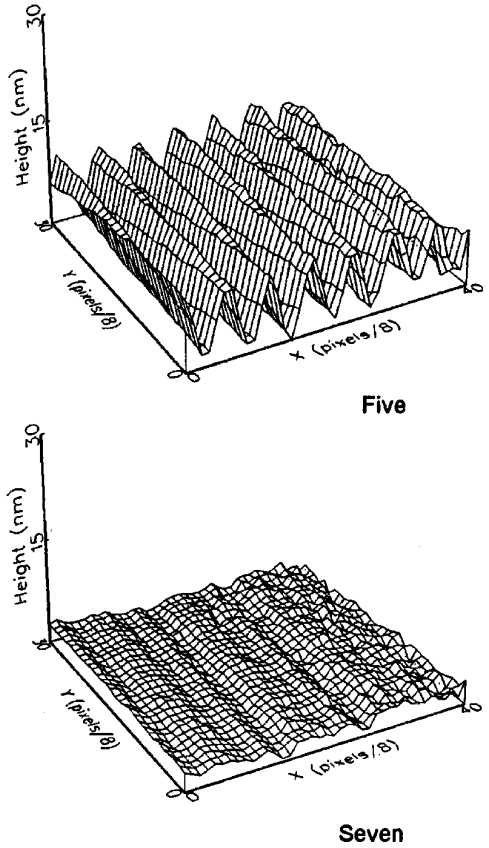

Fig. 7. Experimental surface maps of residual errors when an interferometric microscope was subjected to a 1-Hz vibration having an amplitude equivalent to one-quarter fringe. There were approximately three fringes in the field of view, and the camera frame rate was 25 Hz. The seven-frame algorithm has a greater resistance to low-frequency vibrations than the five-frame algorithm.

rents, air-table oscillations, thermal distortions, and floor motion. Vibration is a serious problem in all interferometers, especially large aperture instruments.

The improvement in vibration sensitivity may be understood qualitatively by thinking of low-frequency vibrations as phase-shift calibration errors. Generally, an error-compensating algorithm should perform well against this kind of environmental disturbance, and in fact the Schwider five-frame algorithm is already much better than three- and four-frame algorithms. However, this qualitative analogy should not be relied on completely, since it is possible to design an algorithm that performs well in the face of calibration errors but overall has poor resistance to vibration.

Experiments with an interferometric microscope have verified the predicted advantages of the new algorithm. Figure 6 shows the experimental variation in P–V system repeatability as a function of calibration error. The repeatability refers to two successive measurements of a smooth, flat part, then calculating the P–V of the difference map. The two measurements are taken at a phase interval of $\pi/2$ in order to isolate the effect of the periodic terms. The experimental data confirm the benefits predicted in Fig. 3. To demonstrate the improved resistance to low-frequency vibration, the microscope has been equipped with two different PZT translators. The first PZT provides the conventional phase-shift ramp, whereas the second introduces additional mechanical vibrations controlled by a waveform generator. Figure 7 shows the results of this test for a 1-Hz vibration, having an amplitude equivalent to one-quarter fringe, using a 25-Hz CCD camera. The seven-frame result is clearly much improved when compared with that of the five-frame algorithm.

5. Conclusion

The theoretical analysis together with experimental work demonstrates the advantages of the new seven-frame algorithm. However, it is expected from the general approach to the derivation of the algorithm that the advantages presented here are not peculiar to the specific number of frames but are rather a general characteristic of PSI algorithms that reasonably approximate a window function designed to reduce leakage in the frequency domain. Thus the same principles can be applied to the derivation of a number of different algorithms of different sizes, with the symmetric seven-frame example representing a good compromise between performance and computing requirements. It is also worth noting that the Von Hann window was chosen for this study because it is relatively easy to calculate. More complicated windows can provide even better performance.

I acknowledge the support of the software engineers here at Zygo in the implementation and testing of the new algorithm. In particular, I thank Toni-Lynn Miles for performing the difficult experiments

that led to Figs. 6 and 7. These experiments require the accurate measurement of small residual errors in data plots and require skill and patience to perform.

References

1. J. E. Greivenkamp and J. H. Bruning, "Phase shifting interferometry," in *Optical Shop Testing*, D. Malacara, ed. (Wiley, New York, 1992), Chap. 14.
2. P. Hariharan, *Optical Interferometry* (Academic, Orlando, Fla., 1985).
3. K. Creath, "Comparison of phase-measurement algorithms," in *Surface Characterization and Testing*, K. Creath, ed., Proc. Soc. Photo-Opt. Instrum. Eng. **680,** 19–28 (1986).
4. J. Schwider, R. Burow, K.-E. Elssner, J. Grzanna, R. Spolaczyk, and K. Merkel, "Digital wavefront measuring interferometry: some systematic error sources," Appl. Opt. **22,** 3421–3432 (1983).
5. P. Hariharan, B. F. Oreb, and T. Eiju, "Digital phase-shifting interferometry: a simple error-compensating phase calculation algorithm," Appl. Opt. **26,** 2504–2506 (1987).
6. J. Schmit and K. Creath, "Some new error-compensating algorithms for phase-shifting interferometry," in *Optical Fabrication and Testing Workshop*, Vol. 13 of OSA 1994 Technical Digest Series (Optical Society of America, Washington, D.C., 1994), Postdeadline paper PD4.
7. K. Freischlad and C. L. Koliopoulos, "Fourier description of digital phase-measuring interferometry," J. Opt. Soc. Am. A **7,** 542–551 (1990).
8. K. G. Larkin and B. F. Oreb, "Design and assessment of symmetrical phase-shifting algorithms," J. Opt. Soc. Am. A **9,** 1740–1748 (1992).
9. J. H. Bruning, D. R. Herriott, J. E. Gallagher, D. P. Rosenfeld, A. D. White, and D. J. Brangaccio, "Digital wavefront measuring interferometer for testing optical surfaces and lenses," Appl. Opt. **13,** 2693–2703 (1974).
10. R. P. Grosso and R. Crane, Jr., "Precise optical evaluation using phase measuring interferometric techniques," in *Interferometry*, G. W. Hopkins, ed., Proc. Soc. Photo-Opt. Instrum. Eng. **192,** 65–74 (1979).
11. P. de Groot, "Phase-shift calibration errors in interferometers with spherical Fizeau cavities," Appl. Opt. **34,** 2856–2863 (1995).
12. F. J. Harris, "On the use of windows for harmonic analysis with the discrete Fourier transform," Proc. IEEE **66,** 51–83 (1978).
13. C. S. Williams, *Designing Digital Filters* (Prentice-Hall, Englewood Cliffs, N.J., 1986), Chap. 4.
14. K. Creath and P. Hariharan, "Phase-shifting errors in interferometric tests with high-numerical aperture reference surfaces," Appl. Opt. **33,** 24–25 (1994).
15. P. de Groot and L. Deck, "Long-wavelength laser diode interferometer for surface flatness measurement," in *Optical Measurements and Sensors for the Process Industries*, C. Gorecki, ed., Proc. Soc. Photo-Opt. Instrum. Eng. **2248,** 136–140 (1994).
16. J. van Wingerden, H. J. Frankena, and C. Smorenburg, "Linear approximation for measurement errors in phase shifting interferometry," Appl. Opt. **30,** 2718–2729 (1991).
17. P. de Groot, "Predicting the effects of vibration in phase shifting interferometry," in *Optical Fabrication and Testing Workshop*, Vol. 13 of OSA 1994 Technical Digest Series (Optical Society of America, Washington, D.C., 1994), pp. 189–192.
18. P. de Groot, "Vibration in phase-shifting interferometry," J. Opt. Soc. Am. A **12,** 354–365 (1995).